

Determination of astrophysical $^{12}\text{N}(p, \gamma)^{13}\text{O}$ reaction rate from the $^2\text{H}(^{12}\text{N}, ^{13}\text{O})n$ reaction and its astrophysical implications

B. Guo, J. Su, Z. H. Li, Y. B. Wang, S. Q. Yan, Y. J. Li, N. C. Shu, Y. L. Han, X. X. Bai, Y. S. Chen, and W. P. Liu*
China Institute of Atomic Energy, P.O. Box 275(10), Beijing 102413, China

H. Yamaguchi, D. N. Binh, T. Hashimoto, S. Hayakawa, D. Kahl, and S. Kubono
*Center for Nuclear Study (CNS), the University of Tokyo,
 Wako Branch, 2-1 Hirosawa, Wako, Saitama 351-0198, Japan*

J. J. He, J. Hu, and S. W. Xu
Institute of Modern Physics, Chinese Academy of Sciences (CAS), Lanzhou 730000, China

N. Iwasa and N. Kume
Department of Physics, Tohoku University, 6-6 Aoba, Sendai, Miyagi 980-8578, Japan

Z. H. Li
School of Physics and State Key Laboratory of Nuclear Physics and Technology, Peking University, Beijing 100871, China
 (Dated: November 22, 2012)

The evolution of massive stars with very low-metallicities depends critically on the amount of CNO nuclides which they produce. The $^{12}\text{N}(p, \gamma)^{13}\text{O}$ reaction is an important branching point in the rap-processes, which are believed to be alternative paths to the slow 3α process for producing CNO seed nuclei and thus could change the fate of massive stars. In the present work, the angular distribution of the $^2\text{H}(^{12}\text{N}, ^{13}\text{O})n$ proton transfer reaction at $E_{\text{c.m.}} = 8.4$ MeV has been measured for the first time. Based on the Johnson-Soper approach, the square of the asymptotic normalization coefficient (ANC) for the virtual decay of $^{13}\text{O}_{\text{g.s.}} \rightarrow ^{12}\text{N} + p$ was extracted to be 3.92 ± 1.47 fm $^{-1}$ from the measured angular distribution and utilized to compute the direct component in the $^{12}\text{N}(p, \gamma)^{13}\text{O}$ reaction. The direct astrophysical S-factor at zero energy was then found to be 0.39 ± 0.15 keV b. By considering the direct capture into the ground state of ^{13}O , the resonant capture via the first excited state of ^{13}O and their interference, we determined the total astrophysical S-factors and rates of the $^{12}\text{N}(p, \gamma)^{13}\text{O}$ reaction. The new rate is two orders of magnitude slower than that from the REACLIB compilation. Our reaction network calculations with the present rate imply that $^{12}\text{N}(p, \gamma)^{13}\text{O}$ will only compete successfully with the β^+ decay of ^{12}N at higher (\sim two orders of magnitude) densities than initially predicted.

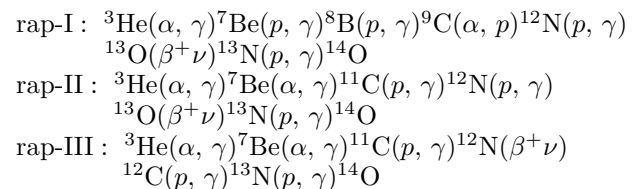
PACS numbers: 25.60.Je; 25.40.Lw; 26.50.+x; 27.20.+n

I. INTRODUCTION

The first generation of stars formed at the end of the cosmic dark ages, which marked the key transition from a homogeneous and simple universe to a highly structured and complex one [1]. The first stars of zero metallicity are so-called Population III that formed before Population I in galactic disks and Population II in galactic halos [2, 3]. The most fundamental question about Population III stars is how massive they typically were since the mass of stars dominates their fundamental properties such as lifetimes, structures and evolutions. Recent numerical simulations of the collapse and fragmentation of primordial gas clouds indicate that these stars are predominantly very massive with masses larger than hundreds of M_{\odot} (see Ref. [1] and references therein).

A classic question on the evolution of supermassive stars is whether they contributed any significant mate-

rial to later generations of stars by supernova explosions which ended the lives of Population III stars. In 1986, Fuller, Woosley and Weaver [4] studied the evolution of non-rotating supermassive stars with a hydrodynamic code KEPLER. They concluded that these stars will collapse into black holes without experiencing a supernova explosion. This is because the triple alpha process ($3\alpha \rightarrow ^{12}\text{C}$) does not produce sufficient amounts of CNO seed nuclei so that the hot CNO cycle and rp -process are unable to generate the nuclear energy enough to explode the stars. In 1989, Wiescher, Görres, Graff et al. [5] suggested the rap-processes as alternative paths which would permit these stars to bypass the 3α process and to yield the CNO material. The reactions involved in the rap-processes are listed as below:



* Corresponding author: wpliu@ciae.ac.cn

rap-IV : ${}^3\text{He}(\alpha, \gamma){}^7\text{Be}(\alpha, \gamma){}^{11}\text{C}(\alpha, p){}^{14}\text{N}(p, \gamma){}^{15}\text{O}$.

It is crucial to determine the rates of the key reactions in the rap-processes in order to study if they play any significant role in the evolution of supermassive stars by producing CNO material. ${}^{12}\text{N}(p, \gamma){}^{13}\text{O}$ is an important reaction in the rap-I and rap-II processes.

Due to the low Q-value (1.516 MeV) of the ${}^{12}\text{N}(p, \gamma){}^{13}\text{O}$ reaction, its stellar reaction rate is dominated by the direct capture into the ground state in ${}^{13}\text{O}$. In addition, the resonant capture via the first excited state in ${}^{13}\text{O}$ could play an important role for determining the reaction rates. In 1989, Wiescher et al. [5] derived the direct astrophysical S-factor at zero energy, $S(0)$, to be ~ 40 keV b based on a shell model calculation. In 2006, Li [6] extracted the direct $S(0)$ factor to be 0.31 keV b by using the spectroscopic factor from the shell model calculation of Ref. [7], where the proton-removal cross section of ${}^{13}\text{O}$ on a Si target was well reproduced. It should be noted that there is a discrepancy of two orders of magnitude between the above two values of the direct $S(0)$ factor. In 2009, Banu, Al-Abdullah, Fu et al. [8] derived the asymptotic normalization coefficient (ANC) for the virtual decay of ${}^{13}\text{O}_{\text{g.s.}} \rightarrow {}^{12}\text{N} + p$ from the measurement of the ${}^{14}\text{N}({}^{12}\text{N}, {}^{13}\text{O}){}^{13}\text{C}$ angular distribution and then calculated the direct $S(0)$ factor to be 0.33 ± 0.04 keV b, which is consistent with that in Ref. [6]. As for the resonant capture component, the resonant parameters of the first excited state in ${}^{13}\text{O}$ have been studied through a thick target technique [9, 10] and R -matrix method [8, 10]. In 1989, Wiescher et al. [5] derived the radiative width to be $\Gamma_\gamma = 24$ meV with one order of magnitude uncertainty based on a Weisskopf estimate of the transition strength. In 2007, Skorodumov, Rogachev, Boutachkov et al. [10] measured the excitation function of the resonant elastic scattering of ${}^{12}\text{N} + p$ and extracted the spin and parity to be $J^\pi = 1/2^+$ for the first excited state in ${}^{13}\text{O}$ via an R -matrix analysis. In addition, the excitation energy and the proton width were determined to be 2.69 ± 0.05 MeV and 0.45 ± 0.10 MeV, respectively. In 2009, Banu et al. [8] derived a radiative width $\Gamma_\gamma = 0.95$ eV by using the experimental ANC, based on the R -matrix approach.

This work aims at determining the astrophysical S-factors and rates of the ${}^{12}\text{N}(p, \gamma){}^{13}\text{O}$ reaction through the ANC approach based on an independent proton transfer reaction. Here, the angular distribution of the ${}^{12}\text{N}(d, n){}^{13}\text{O}$ reaction leading to the ground state in ${}^{13}\text{O}$ is measured in inverse kinematics, and used to extract the ANC for the virtual decay of ${}^{13}\text{O}_{\text{g.s.}} \rightarrow {}^{12}\text{N} + p$ through the Johnson-Soper adiabatic approximation [11]. The (d, n) transfer system has been successfully applied to the study of some proton radiative capture reactions, such as ${}^7\text{Be}(p, \gamma){}^8\text{B}$ [12, 13], ${}^8\text{B}(p, \gamma){}^9\text{C}$ [14], ${}^{11}\text{C}(p, \gamma){}^{12}\text{N}$ [15], and ${}^{13}\text{N}(p, \gamma){}^{14}\text{O}$ [16]. The astrophysical S-factors and rates for the direct capture in the ${}^{12}\text{N}(p, \gamma){}^{13}\text{O}$ reaction are then calculated by using the measured ANC. Finally, we obtain the total S-factors and rates by taking into account the direct capture, the resonant capture and their

interference, and study the temperature-density conditions at which the ${}^{12}\text{N}(p, \gamma){}^{13}\text{O}$ reaction takes place.

II. MEASUREMENT OF THE ${}^2\text{H}({}^{12}\text{N}, {}^{13}\text{O})n$ ANGULAR DISTRIBUTION

The experiment was performed with the CNS low energy in-flight Radio-Isotope Beam (CRIB) separator [17, 18] in the RIKEN RI Beam Factory (RIBF). A ${}^{10}\text{B}$ primary beam with an energy of 82 MeV was extracted from the AVF cyclotron. The primary beam impinged on a ${}^3\text{He}$ gas target with a pressure of 360 Torr and a temperature of 90 K; the target gas was confined in a small chamber with a length of 80 mm [19]. The front and rear windows of the gas chamber are Havar foils, each in a thickness of $2.5 \mu\text{m}$. The secondary ${}^{12}\text{N}$ ions with an energy of 70 MeV were produced through the ${}^3\text{He}({}^{10}\text{B}, {}^{12}\text{N})n$ reaction and then selected by the CRIB separator, which mainly consists of two magnetic dipoles and a velocity filter (Wien filter).

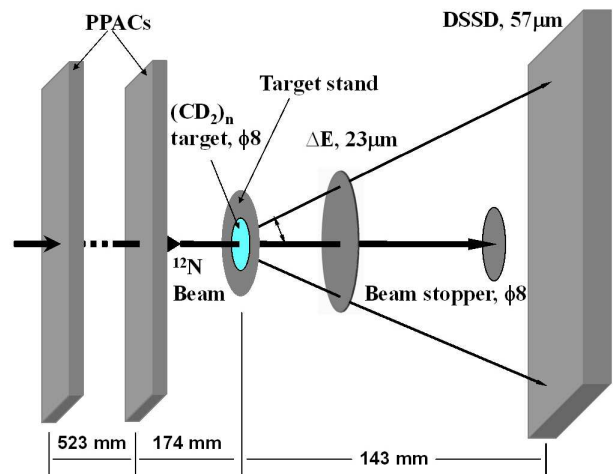


FIG. 1. (Color online) Schematic layout of the experimental setup at the secondary reaction chamber (namely F3 chamber in Ref. [18]) of CRIB for the ${}^2\text{H}({}^{12}\text{N}, {}^{13}\text{O}_{\text{g.s.}})n$ reaction.

A schematic layout of the experimental setup at the secondary reaction chamber (namely F3 chamber, see Ref. [18] for details) of CRIB separator is shown in Fig. 1. The cocktail beam which included ${}^{12}\text{N}$ was measured event-by-event using two parallel plate avalanche counters (PPACs) [20]; in this way, we determined the particle identification, precise timing information, and could extrapolate the physical trajectory of each ion in real space. In Fig. 2 we display the histogram of time of flight (TOF) vs. horizontal position (X) on the upstream PPAC in the F3 chamber for the particle identification of the cocktail beam. The main contaminants are ${}^7\text{Be}$ ions with the similar magnetic rigidities and velocities to the ${}^{12}\text{N}$ ions of interest. After the two PPACs, the ${}^{12}\text{N}$

secondary beam bombarded a deuterated polyethylene (CD_2) film with a thickness of 1.5 mg/cm^2 to study the $^2\text{H}(^{12}\text{N}, ^{13}\text{O})n$ reaction. A carbon film with a thickness of 1.5 mg/cm^2 was utilized to evaluate the background contribution from the carbon nuclei in the (CD_2) target. The target stand with a diameter of 8 mm also served as a beam collimator. The typical purity and intensity of the ^{12}N ions on target were approximately 30% and 500 pps after the collimator, respectively.

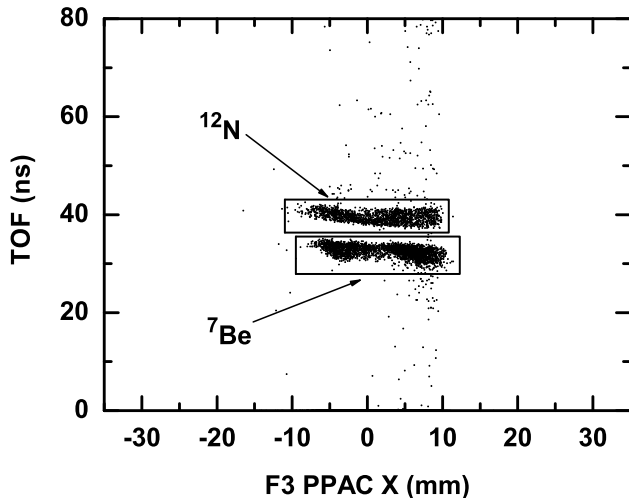


FIG. 2. Two-dimensional histogram of TOF vs. horizontal position (X) on the upstream PPAC in the F3 chamber for the particle identification of the cocktail beam.

The ^{13}O reaction products were detected and identified with a telescope consisting of a $23 \mu\text{m}$ silicon detector (ΔE) and a $57 \mu\text{m}$ double-sided silicon strip detector (DSSD). In order to determine the energy of ^{12}N ions after they pass through two PPACs, a silicon detector with a thickness of $1500 \mu\text{m}$ was placed between the downstream PPAC and the (CD_2) target, and removed after measuring the beam energy. The energy calibration of the detectors was carried out by combining the use of α -source and the magnetic rigidity parameters of ^{10}B and ^{12}N ions. The energy loss of the ^{12}N beam in the whole target was determined from the energy difference measured with and without the target. The ^{12}N beam energy in the middle of the (CD_2) target was derived to be 59 MeV from the energy loss calculation by the program LISE++ [21], which was calibrated by the experimental energy loss in the whole target. In addition, a beam stopper (close to the DSSD) with a diameter of 8 mm was used to block un-reacted beam particles in order to reduce radiation damage to the DSSD.

The emission angles of reaction products were determined by combining the position information from the DSSD and the two PPACs. As an example, Fig. 3 shows a two-dimensional histogram of energy loss (ΔE) vs. residual energy (E_R) for the events in the angular range of $3^\circ < \theta_{\text{c.m.}} < 4^\circ$. For the sake of saving CPU time in

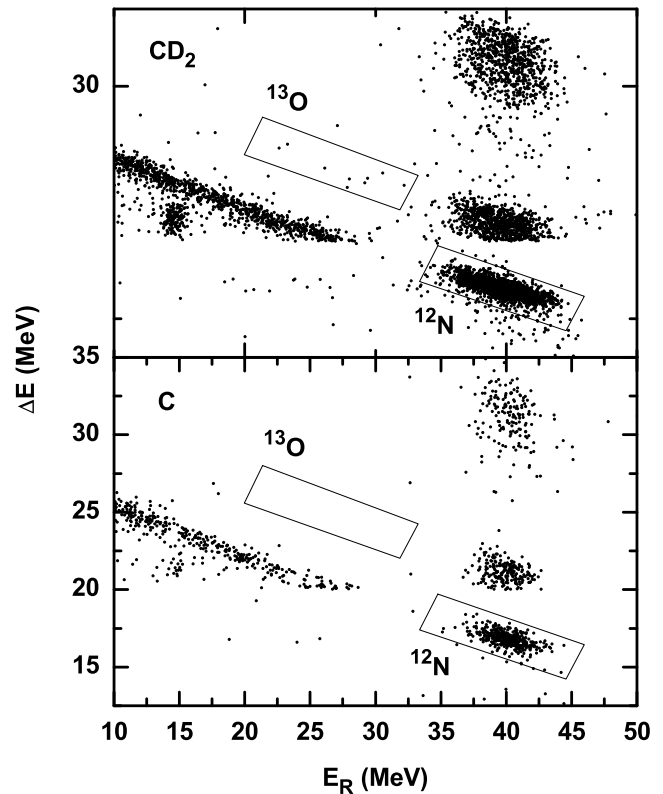


FIG. 3. Two-dimensional histogram of energy loss ΔE vs. residual energy E_R for the events in the angular range of $3^\circ < \theta_{\text{c.m.}} < 4^\circ$. The top and bottom panels display the spectra for the measurement of the deuterated polyethylene (CD_2) and carbon (C) targets, respectively. The two-dimensional cuts for the ^{13}O events from the $^2\text{H}(^{12}\text{N}, ^{13}\text{O})n$ reaction were determined with a MC simulation. See text for details.

dealing with the experimental data, all the events below $\Delta E = 20 \text{ MeV}$ were scaled down by a factor of 100, and the ^{13}O events were not affected. The two-dimensional cuts of the ^{13}O events from the $^2\text{H}(^{12}\text{N}, ^{13}\text{O})n$ reaction were determined with a Monte Carlo (MC) simulation, which took into account the kinematics, geometrical factor, the energy diffusion of the ^{12}N beam, the angular straggling, and the energy straggling in the two PPACs, the secondary target and the ΔE detector. This simulation was calibrated by using the ^{12}N elastic scattering on the target. Such a calibration approach has been successfully used to study the $^2\text{H}(^8\text{Li}, ^9\text{Li})^1\text{H}$ reaction [22]. The ^{13}O events are clearly observed in the two-dimensional cut for the (CD_2) measurement, while no relevant events are observed in this cut for the background measurement. The ^7Be contaminants don't affect the identification of the ^{13}O events since these ions and their products are far from the ^{13}O region in the spectra of ΔE vs. E_R and have significantly different energies from the ^{13}O events. The effects of the pileup of ^7Be with ^{12}N can be estimated and subtracted through the background measurement.

In addition, the detection efficiency correction from the beam stopper was also computed via the MC simulation also by considering the effects mentioned above. The resulting detection efficiencies range from 66% to 100% for different detection regions in the DSSD. After the beam normalization and background subtraction, the angular distribution of the ${}^2\text{H}({}^{12}\text{N}, {}^{13}\text{O}_{\text{g.s.}})n$ reaction in the center of mass frame was obtained and is shown in Fig. 4.

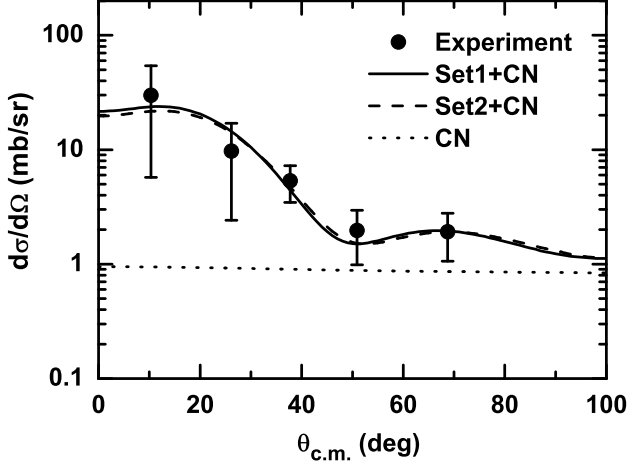


FIG. 4. Measured angular distribution of ${}^2\text{H}({}^{12}\text{N}, {}^{13}\text{O}_{\text{g.s.}})n$ at $E_{\text{c.m.}} = 8.4$ MeV, together with the theoretical calculations on the direct-process contribution using two sets of optical potentials (Set1 and Set2) and the compound-nucleus (CN) contribution. See the text in the section III for the details on the theoretical calculations.

III. ANALYSIS OF THE ${}^2\text{H}({}^{12}\text{N}, {}^{13}\text{O})n$ ANGULAR DISTRIBUTION

For a peripheral transfer reaction, the ANC can be derived by the comparison of the experimental angular distribution with theoretical calculations,

$$\left(\frac{d\sigma}{d\Omega}\right)_{\text{exp}} = \sum_{j_i j_f} (C_{l_i j_i}^d)^2 (C_{l_f j_f}^{13\text{O}})^2 R_{l_i j_i l_f j_f}, \quad (1)$$

where

$$R_{l_i j_i l_f j_f} = \frac{\sigma_{l_i j_i l_f j_f}^{th}}{(b_{l_i j_i}^d)^2 (b_{l_f j_f}^{13\text{O}})^2}. \quad (2)$$

$\left(\frac{d\sigma}{d\Omega}\right)_{\text{exp}}$ and $\sigma_{l_i j_i l_f j_f}^{th}$ are the experimental and theoretical differential cross sections, respectively. $C_{l_f j_f}^{13\text{O}}$, $C_{l_i j_i}^d$ and $b_{l_f j_f}^{13\text{O}}$, $b_{l_i j_i}^d$ represent the nuclear ANCs and the corresponding single particle ANCs for the virtual decays of ${}^{13}\text{O}_{\text{g.s.}} \rightarrow {}^{12}\text{N} + p$ and $d \rightarrow p + n$, respectively. l_i , j_i and l_f , j_f denote the orbital and total angular momenta of the transferred proton in the initial and final nuclei d

TABLE I. Optical potential parameters used in the calculation, where V and W are in MeV, r and a in fm.

Set No.	1 [24]	2 [25]		
Channel	Entrance	Exit	Entrance	Exit
V_r	97.03	53.44	99.84	55.44
r_{0r}	1.152	1.154	1.127	1.131
a_r	0.722	0.69	0.708	0.676
W	1.73		0.86	0.77
r_w	1.693		1.693	1.131
a_w	0.716		0.711	0.676
W_s	14.01	9.61	14.2	9.54
r_{0s}	1.147	1.147	1.306	1.306
a_s	0.716	0.716	0.56	0.56
V_{so}	5.9	5.9	5.65	5.65
r_{0so}	0.816	0.83	0.903	0.907
a_{so}	0.661	0.63	0.622	0.622
r_{0c}	1.25		1.25	

and ${}^{13}\text{O}$, respectively. $R_{l_i j_i l_f j_f}$ is model independent in the case of a peripheral transfer reaction; therefore, the extraction of the ANC is insensitive to the geometric parameters (radius r_0 and diffuseness a) of the bound state potential.

In this work, the code FRESKO [23] was used to analyze the experimental angular distribution. In order to include the breakup effects of deuterons in the entrance channel, the angular distribution was calculated within the Johnson-Soper adiabatic approximation to the neutron, proton, and target three-body system [11]. In the present calculation, the optical potentials of nucleon-target were taken from Refs. [24, 25], which have been successfully applied to the study of some of the reactions on light nuclei [26–28]. The theoretical angular distributions of the direct process were calculated with these two sets of optical potentials, as shown in Fig. 4. The employed optical potential parameters are listed in Table I. In addition, the UNF code [29] was used to evaluate the compound-nucleus (CN) contribution in the ${}^2\text{H}({}^{12}\text{N}, {}^{13}\text{O}_{\text{g.s.}})n$ reaction, as indicated by the dotted line in Fig. 4. The single-particle bound state wave functions were calculated with conventional Woods-Saxon potentials whose depths were adjusted to reproduce the binding energies of the proton in the ground states of the deuteron ($E_b = 2.225$ MeV) and ${}^{13}\text{O}$ ($E_b = 1.516$ MeV). To verify if the transfer reaction is peripheral, the ANCs and the spectroscopic factors were computed by changing the geometric parameters of Woods-Saxon potential for single-particle bound state, using one set of the optical potential, as displayed in Fig. 5. One sees that the spectroscopic factors depend significantly on the selection of the geometric parameters, while the ANC is nearly constant, indicating that the ${}^2\text{H}({}^{12}\text{N}, {}^{13}\text{O}_{\text{g.s.}})n$ reaction at the present energy is dominated by the peripheral process.

The spins and parities of ${}^{12}\text{N}_{\text{g.s.}}$ and ${}^{13}\text{O}_{\text{g.s.}}$ are 1^+ and $3/2^-$, respectively. Therefore, the ${}^2\text{H}({}^{12}\text{N}, {}^{13}\text{O}_{\text{g.s.}})n$

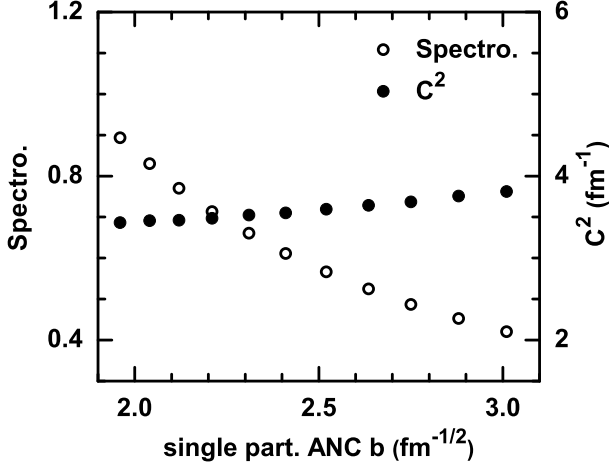


FIG. 5. Variation of the spectroscopic factor (Spectro.) and the square of the ANC (C^2) for the virtual decay of $^{13}\text{O}_{\text{g.s.}} \rightarrow ^{12}\text{N} + p$ as a function of the single particle ANC b .

cross section could include two contributions from the proton transfers to $1p_{3/2}$ and $1p_{1/2}$ orbits in ^{13}O . The ratio of $1p_{3/2}:1p_{1/2}$ $[(C_{p_{3/2}}^{13\text{O}})^2/(C_{p_{1/2}}^{13\text{O}})^2]$ was derived to be 0.16 based on a shell model calculation [7]. C_d^2 was taken to be 0.76 fm^{-1} from Ref. [30]. After the subtraction of the CN contribution, the first three data points at forward angles were used to derive the ANC by the comparison of the experimental data with the theoretical calculations. For one set of optical potential, three ANCs can be obtained by using three data points, and their weighted mean was then taken as the final value. The square of the ANCs for the $1p_{1/2}$ and $1p_{3/2}$ orbits were extracted to be $(C_{p_{1/2}}^{13\text{O}})^2 = 3.38 \pm 1.27 \text{ fm}^{-1}$ and $(C_{p_{3/2}}^{13\text{O}})^2 = 0.54 \pm 0.20 \text{ fm}^{-1}$, respectively. Consequently, the square of total ANC was $(C_{\text{tot}}^{13\text{O}})^2 = 3.92 \pm 1.47 \text{ fm}^{-1}$. The error resulted from the measurement (36%) and the uncertainty of the optical potentials (12%). This result is in agreement with the value of $(C_{p_{1/2}}^{13\text{O}})^2 = 2.53 \pm 0.30 \text{ fm}^{-1}$ obtained from the $^{14}\text{N}(^{12}\text{N}, ^{13}\text{O})^{13}\text{C}$ reaction [8].

IV. ASTROPHYSICAL RATE OF THE $^{12}\text{N}(p, \gamma)^{13}\text{O}$ REACTION AND ITS ASTROPHYSICAL IMPLICATIONS

The ANC, which defines the amplitude of the tail of the radial overlap function, determines the overall normalization of the direct astrophysical S-factors [31]. In the present work, the direct capture cross sections and astrophysical S-factors were computed based on the measured ANC by using the RADCAP code [32], which is a potential model tool for direct capture reactions. The resulting direct astrophysical S-factors as a function of $E_{\text{c.m.}}$ are displayed in Fig. 6, as indicated by the dashed

line. The S-factor at zero energy was then found to be $S(0) = 0.39 \pm 0.15 \text{ keV b}$, which agrees with the values in Refs. [6, 8].

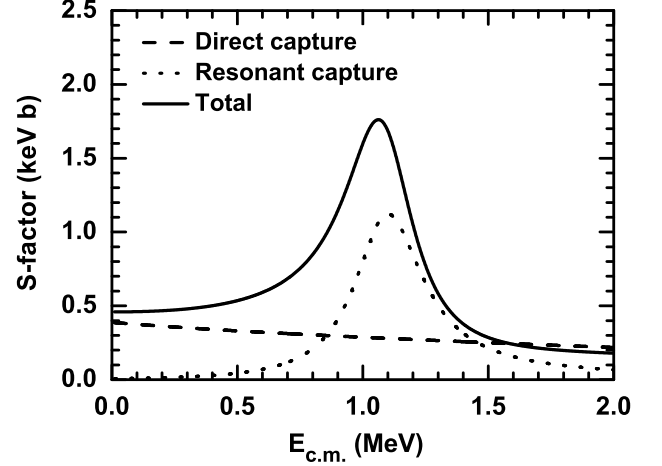


FIG. 6. Astrophysical S-factors of the $^{12}\text{N}(p, \gamma)^{13}\text{O}$ reaction as a function of $E_{\text{c.m.}}$. The dashed and dotted curves represent the direct and resonant components, respectively. The solid curve denotes the total S-factor. See text for details.

The astrophysical S-factors of the resonant capture can be obtained by using Breit-Wigner formula. In the present calculation, the resonant parameters ($J^\pi = 1/2^+$, $E_x = 2.69 \pm 0.05 \text{ MeV}$, $\Gamma_p = 0.45 \pm 0.10 \text{ MeV}$ [10], and $\Gamma_\gamma = 0.95 \pm 0.24 \text{ eV}$ [8]) were adopted. In Fig. 6, we display the resulting S-factors for the resonant capture, as indicated by the dotted line.

Interference effects will occur only in the case that the resonant and direct amplitudes have the same channel spin I and the same incoming orbital angular momentum [8, 33]. The direct capture amplitude for the $^{12}\text{N}(p, \gamma)^{13}\text{O}$ reaction is given by the sum of $I = 1/2$ and $3/2$ components. Since the channel spin for the first resonance is $1/2$, only the first component in the direct capture interferes with the resonant amplitude. Therefore, the total S-factors were calculated with

$$S_t(E) = S_d(E) + S_r(E) \pm 2[S_d^{1/2}(E)S_r(E)]^{1/2} \cos(\delta), \quad (3)$$

where $S_d(E)$, $S_r(E)$ and $S_d^{1/2}(E)$ denote the astrophysical S-factors for the direct capture, the resonant capture, and the $I=1/2$ component in the direct capture, respectively. δ is the resonance phase shift, which can be given by

$$\delta = \arctan \left[\frac{\Gamma_p(E)}{2(E - E_R)} \right]. \quad (4)$$

Here, $\Gamma_p(E) = \Gamma_p \frac{P_{I_i}(E)}{P_{I_i}(E_R)}$, where $P_{I_i}(E)$ is the penetration factor. The ratio of the $I=1/2$ amplitude to the total amplitude in the direct capture was derived to be $2/3$ using the RADCAP code. Generally, the sign of

the interference in Equation 3 has to be determined experimentally. However, it is also possible to infer this sign via an R -matrix method. Recently, Banu et al. [8] found the constructive interference below the resonance and the destructive one above it using an R -matrix approach. Based on this interference pattern, the present total S-factors were then obtained, as shown in Fig. 6. In addition, we estimated the uncertainty of the total S-factors by taking into account the errors of the present ANC for the ground state in ^{13}O and the employed resonant parameters for the first excited state in ^{13}O .

The astrophysical $^{12}\text{N}(p, \gamma)^{13}\text{O}$ reaction rates ($\text{cm}^3\text{s}^{-1}\text{mol}^{-1}$) were then calculated with [34, 35]

$$N_A \langle \sigma v \rangle = N_A \left(\frac{8}{\pi \mu} \right)^{1/2} \frac{1}{(kT)^{3/2}} \int_0^\infty S(E) \exp \left[- \left(\frac{E_G}{E} \right)^{1/2} - \frac{E}{kT} \right] dE, \quad (5)$$

where the Gamow energy $E_G = 0.978 Z_1^2 Z_2^2 \mu$ MeV, and N_A is Avogadro's number.

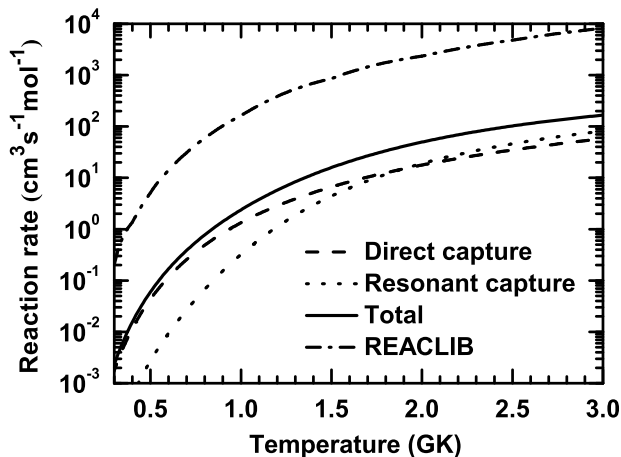


FIG. 7. Astrophysical rates of the $^{12}\text{N}(p, \gamma)^{13}\text{O}$ reaction as a function of temperature. The dashed and dotted curves represent the present rates of the direct and resonant captures, respectively. The solid curve represents the total rates in the present work, while the dash-dotted curve denotes the REACLIB compilation [5]. See text for details.

In Fig. 7 we display the resulting reaction rates as a function of temperature, together with the REACLIB compilation [5]. There is a discrepancy of up to a factor of ~ 100 between these two reaction rates for the temperatures below $T_9 = 3$ (T_9 is a temperature in unit of 10^9 K). In addition, our total rates are in good agreement with those in Fig. 9 of Ref. [8] since the similar contribution of the direct capture was found and the same resonant parameters were used in both works. From Fig. 7 one also sees that the direct capture dominates the $^{12}\text{N}(p, \gamma)^{13}\text{O}$ reaction for the temperatures below $T_9 = 1.5$.

TABLE II. The coefficients a_i in Eq. 6 for the central value, lower limit and upper limit of the $^{12}\text{N}(p, \gamma)^{13}\text{O}$ reaction rate. The fitting errors are all less than 6% at $T_9 = 0.01$ -10.

a_i	Central value	Upper limit	Lower limit
a_1	-5.91219	-3.77150	-4.48818
a_2	0.0400148	0.0224401	0.0253469
a_3	-22.2259	-20.3542	-20.5376
a_4	32.2983	28.2893	28.6331
a_5	-3.56352	-3.29024	-3.36174
a_6	0.261761	0.243627	0.252225
a_7	-10.1115	-8.37104	-8.49396
a_8	-10.0637	4.00598	-7.05380
a_9	-0.553380	0.190095	-0.291547
a_{10}	-20.7778	-31.6274	-20.5490
a_{11}	31.5635	31.0575	27.9040
a_{12}	-3.64300	-6.70434	-3.31062
a_{13}	0.248400	-0.399390	0.244458
a_{14}	-12.2610	-13.7936	-10.4292

We fitted the new rates with an expression used in the astrophysical reaction rate library REACLIB [36, 37]. The total reaction rates were fitted as

$$N_A \langle \sigma v \rangle = \exp[a_1 + a_2 T_9^{-1} + a_3 T_9^{-1/3} + a_4 T_9^{1/3} + a_5 T_9 + a_6 T_9^{5/3} + a_7 \ln(T_9)] + \exp[a_8 + a_9 T_9^{-1} + a_{10} T_9^{-1/3} + a_{11} T_9^{1/3} + a_{12} T_9 + a_{13} T_9^{5/3} + a_{14} \ln(T_9)]. \quad (6)$$

The coefficients a_i for the central value, lower limit and upper limit of the $^{12}\text{N}(p, \gamma)^{13}\text{O}$ reaction rate are listed in Table II. The fitting errors are all less than 6% in a range from $T_9 = 0.01$ to $T_9 = 10$.

Since there is the large discrepancy between the rates in this work and those in Ref. [5], the temperature and density conditions at which the rap-processes are expected to operate need to be revised. We performed reaction network simulations with a series of constant temperatures (0.1-1.5 GK) and densities (1 - 10^8 g/cm 3), and a burning time of 100 s, and primordial abundances and reaction rates from REACLIB as an initial input.

In Fig. 8 we shows the resulting temperature-density conditions for the rap-I,II and rap-III processes by using the present $^{12}\text{N}(p, \gamma)^{13}\text{O}$ rates and those of Ref. [5]. Curve 1 indicates the present conditions at which the $^{12}\text{N}(p, \gamma)^{13}\text{O}$ reaction has equal strength with the competing β^+ decay of ^{12}N . Below this curve, the ^{12}N β^+ decay will prevail over its proton capture and lead to ^{12}C . Curve 2 shows the same result determined from Ref. [5]. In Regions 3-6, more than 10^{-6} abundances (mass fraction/mass number) could be converted to CNO cycle. One sees that the present region for rap-I and rap-II (Region 3), where the $^{12}\text{N}(p, \gamma)^{13}\text{O}$ reaction operates, was significantly reduced relative to that from the compilation (Region 5). Therefore, the lower limit of the density, where the 10^{-6} abundance can be converted to CNO cycle, was raised from ~ 10 to ~ 1000 g/cm 3 . This

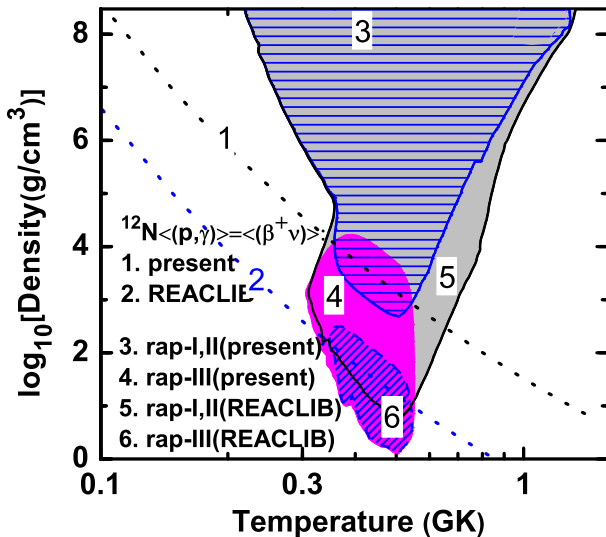


FIG. 8. (Color online) Temperature and density conditions at which the $^{12}\text{N}(p, \gamma)^{13}\text{O}$ reaction could operate. Curve 1 represents the equilibrium lines between the rates of the $^{12}\text{N}(p, \gamma)^{13}\text{O}$ reaction and $^{12}\text{N} \beta^+$ decay. Curve 2 shows the same result determined from Ref. [5]. Regions 3 and 4 denote the revised temperature-density conditions for rap-I,II and rap-III with the present $^{12}\text{N}(p, \gamma)^{13}\text{O}$ rate, respectively, while Regions 5 and 6 represent those with the REACLIB rate from Ref. [5]. Within these four regions more than 1×10^{-6} abundance (mass fraction/mass number) could be converted to CNO cycle. Note that when determining Regions 3 and 4, only the $^{12}\text{N}(p, \gamma)^{13}\text{O}$ rate was changed, all the rest were still taken from the REACLIB compilations.

is because the new rates are about two orders of magnitude slower than the compilation. On the contrary, the present region for rap-III (Region 4), where the β -decay of ^{12}N prevails over its proton capture, was enlarged relative to Region 6, which led to an increase of the upper limit of the density from ~ 100 to $\sim 10000 \text{ g/cm}^3$.

In brief, the present rate of $^{12}\text{N}(p, \gamma)^{13}\text{O}$ shows that it will only compete successfully with the β^+ decay of ^{12}N at higher (\sim two orders of magnitude) densities than initially predicted in Ref. [5]. This finding is consistent with the result reported in Ref. [8], while is contrary to that in Ref. [10].

V. SUMMARY AND CONCLUSION

In this work, the angular distribution of the $^2\text{H}(^{12}\text{N}, ^{13}\text{O}_{\text{g.s.}})n$ reaction was measured and utilized to derive the ANC for the virtual decay of $^{13}\text{O}_{\text{g.s.}} \rightarrow ^{12}\text{N} + p$. Our result is in agreement with that from the $^{14}\text{N}(^{12}\text{N}, ^{13}\text{O})^{13}\text{C}$ transfer reaction in Ref. [8]. The astrophysical S-factors and rates for the direct capture in the $^{12}\text{N}(p, \gamma)^{13}\text{O}$ reaction were then obtained from the measured ANC by using the direct radiative capture model. In addition, we determined the total S-factors and reaction rates by taking into account the direct capture into the ground state of ^{13}O , the resonant capture via the first excited state of ^{13}O and the interference between them. This work provides an independent examination to the existing results on the $^{12}\text{N}(p, \gamma)^{13}\text{O}$ reaction. We conclude that the direct capture dominates the $^{12}\text{N}(p, \gamma)^{13}\text{O}$ reaction for the temperatures below $T_9 = 1.5$.

We also performed reaction network simulations with the new rates. The results imply that $^{12}\text{N}(p, \gamma)^{13}\text{O}$ will only compete successfully with the $^{12}\text{N} \beta^+$ decay at higher (\sim two orders of magnitude) densities than initially predicted in Ref. [5]. Recent simulation of massive metal-free stars between 120 and 1000 solar masses shows that a metallicity as small as $\sim 1 \times 10^{-9}$ is sufficient to stop the contraction [38]. Therefore, this revise of temperature-density conditions may have substantial implications on the evolution of these massive metal-free stars.

ACKNOWLEDGMENTS

We acknowledge the staff of AVF accelerator for the smooth operation of the machine. We thank the anonymous referee for the helpful comments. This work was supported by the National Natural Science Foundation of China under Grant Nos. 11021504, 10875175, 10720101076, 10975193 and 11075219, the 973 program under Grant No. 2013CB834406, KAKEHI of Japan under Grant No. 21340053.

[1] V. Bromm and R. B. Larson, *Annu. Rev. Astron. Astrophys.* **42**, 79 (2004).
 [2] R. Cayrel, *Astron. Astrophys.* **168**, 81 (1986).
 [3] B. J. Carr, *Nature* **326**, 829 (1987).
 [4] G. M. Fuller, S. E. Woosley, and T. A. Weaver, *Astrophys. J.* **307**, 675 (1986).
 [5] M. Wiescher, J. Görres, S. Graff, L. Buchmann, and F.-K. Thielemann, *Astrophys. J.* **343**, 352 (1989).
 [6] Z. H. Li, *Chin. Phys. Lett.* **23**, 3219 (2006).
 [7] R. E. Warner, F. Carstoiu, J. A. Brown, F. D. Becchetti,

D. A. Roberts, B. Davids, A. Galonsky, R. M. Ronnigen, M. Steiner, M. Horoi, J. J. Kolata, A. Nadasen, C. Samanta, J. Schwartzberg, and K. Subotic, *Phys. Rev. C* **74**, 014605 (2006).
 [8] A. Banu, T. Al-Abdullah, C. Fu, C. A. Gagliardi, M. McCleskey, A. M. Mukhamedzhanov, G. Tabacaru, L. Trache, R. E. Tribble, Y. Zhai, F. Carstoiu, V. Burjan, and V. Kroha, *Phys. Rev. C* **79**, 025805 (2009).
 [9] T. Teranishi, S. Kubono, S. Shimoura, M. Notani, Y. Yanagisawa, S. Michimasa, K. Ue, H. Iwasaki, M.

- Kurokawa, Y. Satou, T. Morikawa, A. Saito, H. Baba, J. H. Lee, C. S. Lee, Zs. Fülöp, and S. Kato, Nucl. Phys. A **718**, 207c (2003).
- [10] B. B. Skorodumov, G. V. Rogachev, P. Boutachkov, A. Aprahamian, V. Z. Goldberg, A. Mukhamedzhanov, S. Almaraz, H. Amro, F. D. Becchetti, S. Brown, Y. Chen, H. Jiang, J. J. Kolata, L. O. Lamm, M. Quinn, and A. Woehr, Phys. Rev. C **75**, 024607 (2007).
- [11] G. L. Wales and R. C. Johnson, Nucl. Phys. A **274**, 168 (1976).
- [12] W. Liu, X. Bai, S. Zhou, Z. Ma, Z. Li, Y. Wang, A. Li, Z. Ma, B. Chen, X. Tang, Y. Han, and Q. Shen, Phys. Rev. Lett. **77**, 611 (1996).
- [13] J. J. Das, V. M. Datar, P. Sugathan, N. Madhavan, P. V. Madhusudhana Rao, A. Jhingan, A. Navin, S. K. Dhimman, S. Barua, S. Nath, T. Varughese, A. K. Sinha, R. Singh, A. Ray, D. L. Sastry, R. G. Kulkarni, and R. Shyam, Phys. Rev. C **73**, 015808 (2006).
- [14] D. Beaumel, T. Kubo, T. Teranishi, H. Sakurai, S. Fortier, A. Mengoni, N. Aoi, N. Fukuda, M. Hirai, N. Imai, H. Iwasaki, H. Kumagai, H. Laurent, S.M. Lukyanov, J.M. Maison, T. Motobayashi, T. Nakamura, H. Ohnuma, S. Pita, K. Yoneda, and M. Ishihara, Phys. Lett. B **514**, 226 (2001).
- [15] W. Liu, Z. Li, X. Bai, B. Guo, S. Zeng, Y. Chen, S. Yan, B. Wang, G. Lian, Y. Lu, K. Wu, and N. Shu, Nucl. Phys. A **728**, 275 (2003).
- [16] Z. H. Li, B. Guo, S. Q. Yan, G. Lian, X. X. Bai, Y. B. Wang, S. Zeng, J. Su, B. X. Wang, W. P. Liu, N. C. Shu, Y. S. Chen, H. W. Chang, and L. Y. Jiang, Phys. Rev. C **74**, 035801 (2006).
- [17] S. Kubono, Y. Yanagisawa, T. Teranishi, S. Kato, T. Kishida, S. Michimasa, Y. Ohshiro, S. Shimoura, K. Ue, S. Watanabe, and N. Yamazaki, Eur. Phys. J. A **13**, 217 (2002).
- [18] Y. Yanagisawa, S. Kubono, T. Teranishi, K. Ue, S. Michimasa, M. Notani, J.J. He, Y. Ohshiro, S. Shimoura, S. Watanabe, N. Yamazaki, H. Iwasaki, S. Kato, T. Kishida, T. Morikawa, and Y. Mizo, Nucl. Instrum. Methods Phys. Res. Sect. A **539**, 74 (2005).
- [19] H. Yamaguchi, Y. Wakabayashi, G. Amadio, S. Hayakawa, H. Fujikawa, S. Kubono, J. J. He, A. Kim, and D. N. Binh, Nucl. Instrum. Methods Phys. Res. Sect. A **589**, 150 (2008).
- [20] H. Kumagai, A. Ozawa, N. Fukuda, K. Summerer, and I. Tanihata, Nucl. Instrum. Methods Phys. Res. Sect. A **470**, 562 (2001).
- [21] O. B. Tarasov and D. Bazin, Nucl. Instrum. Methods Phys. Res. Sect. B **266**, 4657 (2008).
- [22] B. Guo, Z. H. Li, W. P. Liu, X. X. Bai, G. Lian, S. Q. Yan, B. X. Wang, S. Zeng, J. Su, and Y. Lu, Nucl. Phys. A **761**, 162 (2005).
- [23] I. J. Thompson, Comput. Phys. Rep. **7**, 167 (1988).
- [24] R. L. Varner, W. J. Thompson, T. L. McAbee, E. J. Ludwig, and T. B. Clegg, Phys. Rep. **201**, 57 (1991).
- [25] A. J. Koning and J. P. Delaroche, Nucl. Phys. A **713**, 231 (2003).
- [26] M. B. Tsang, Jenny Lee, and W. G. Lynch, Phys. Rev. Lett. **95**, 222501 (2005).
- [27] X. D. Liu, M. A. Famiano, W. G. Lynch, M. B. Tsang, and J. A. Tostevin, Phys. Rev. C **69**, 064313 (2004).
- [28] B. Guo, Z. H. Li, W. P. Liu, and X. X. Bai, J. Phys. G: Nucl. Part. Phys. **34**, 103 (2007).
- [29] J. Zhang, Nucl. Sci. Eng. **142**, 207 (2002).
- [30] L. D. Blokhintsev, I. Borbely, and E. I. Dolinskii, Sov. J. Part. Nucl. **8**, 485 (1977).
- [31] A. M. Mukhamedzhanov, C. A. Gagliardi, and R. E. Tribble, Phys. Rev. C **63**, 024612 (2001).
- [32] C. A. Bertulani, Comput. Phys. Commun. **156**, 123 (2003).
- [33] A. M. Mukhamedzhanov, A. Azhari, V. Burjan, C. A. Gagliardi, V. Kroha, A. Sattarov, X. Tang, L. Trache, and R. E. Tribble, Nucl. Phys. A **725**, 279 (1999).
- [34] C. E. Rolfs and W. S. Rodney, *Cauldrons in the Cosmos* (The University of Chicago Press, Chicago 1988).
- [35] C. Iliadis, *Nuclear Physics of Stars* (WILEY-VCH Verlag GmbH & Co. KGaA, Weinheim 2007).
- [36] F.-K. Thielemann, M. Arnould, and J. Truran, *Advances in Nuclear Astrophysics*, ed. A. Vangioni-Flam (Gif-sur-Yvette: Editions Frontière), 525 (1987).
- [37] T. Rauscher and F.-K. Thielemann, At. Data Nucl. Data Tables **79**, 47 (2001).
- [38] A. Heger, S. E. Woosley, I. Baraffe, and T. Abel, in *Proceeding of the Mpa/Eso/Mpe/Usm Joint Astronom Conference on Lighthouses of the Universe: The Most Luminous Celestial Objects and Their Use for Cosmology*, edited by M. Gilfanov, R. Sunyaev, and E. Churazov (Springer-Verlag, Berlin, 2002), p. 369.